universe

IMPACT FACTOR 2.6

CITESCORE 5.2

Review

Blazars as Probes for Fundamental Physics

Giorgio Galanti

Special Issue
Multi-wavelength Properties of Active Galactic Nuclei

Edited by
Prof. Stefano Vercellone

MDPI

https://doi.org/10.3390/universe11100327

universe

MDPI

Review

Blazars as Probes for Fundamental Physics

Giorgio Galanti

INAF, Istituto di Astrofisica Spaziale e Fisica Cosmica di Milano, Via A. Corti 12, 20133 Milano, Italy; gam.galanti@gmail.com

Abstract

Blazars are a class of active galactic nuclei characterized by having one of their relativistic jets oriented close to our line of sight. Their broad emission spectrum makes them exceptional laboratories for probing fundamental physics. In this review, we explore the potential impact on blazar observations of three scenarios beyond the standard paradigm: (i) the hadron beam model, (ii) the interaction of photons with axion-like particles (ALPs), and (iii) Lorentz invariance violation. We focus on the very-high-energy spectral features these scenarios induce in the blazars Markarian 501 and 1ES 0229+200, making them ideal targets for testing such effects. Additionally, we examine ALP-induced effects on the polarization of UV-X-ray and high-energy photons from the blazar OJ 287. The unique signatures produced by these models are accessible to current and upcoming instruments—such as the ASTRI Mini Array, CTAO, LHAASO, IXPE, COSI, and AMEGO—offering new opportunities to probe and constrain fundamental physics through blazar observations.

Keywords: blazars; particle physics; astroparticle physics; hadron beam; axion-like particles; Lorentz invariance violation; photon polarization

1. Introduction

The search for new particles, interactions, and extensions of the Standard Model (SM) of particle physics is one of the most important and exciting frontiers in both physics and astrophysics, with the ultimate goal of understanding the fundamental laws that govern our Universe. Examples include dark matter and dark energy, which are believed to constitute the largest part of our Universe, but whose nature and behavior remain unknown, and their detection is still elusive. The astrophysical environment, with its extremely high energies unattainable in laboratory experiments, provides a unique opportunity to explore new physics. In particular, blazars—a type of active galactic nuclei (AGNs)—represent one of the best astrophysical sources for this purpose, as they can emit photons with energies E detectable even above 10 TeV.

Specifically, radio-loud AGN are extragalactic, accreting supermassive black holes (SMBHs), whose main feature is the presence of two collimated relativistic jets emitted in opposite directions. The different AGN phenomenology is fundamentally defined by the viewing angle under which the AGN is seen from Earth [1]. In particular, AGN with jets oriented close to our line of sight are classified as blazars, whereas those with misaligned jets are referred to as radio galaxies. Blazars are further divided into two subclasses: (i) flat spectrum radio quasars (FSRQs) and (ii) BL Lacertae objects (BL Lacs). FSRQs are characterized by strong optical emission lines, attributed to photoionized gas clouds surrounding the central SMBH. They are also highly powerful sources thought to be powered by an efficient accretion disc. Moreover, very-high-energy (VHE) photons in

check for updates

Academic Editor: Nico Cappelluti

Received: 6 August 2025
Revised: 16 September 2025
Accepted: 20 September 2025
Published: 27 September 2025

Citation: Galanti, G. Blazars as Probes for Fundamental Physics. *Universe* **2025**, *11*, 327. https://doi.org/10.3390/universe11100327

FSRQs experience strong absorption due to interactions with photons from the broad-line region (BLR) and the dusty torus via the $\gamma\gamma \to e^+e^-$ process [2]. In contrast, BL Lacs are less powerful, do not exhibit prominent emission lines, likely due to a radiatively inefficient accretion flow that fails to ionize the gas surrounding the SMBH efficiently [3,4], and do not show strong absorption regions for VHE photons. As a consequence, their spectra can typically extend beyond 10 TeV, making BL Lacs particularly suitable for probing fundamental physics at VHE.

The emission from blazars (both FSRQs and BL Lacs) spans a broad energy range, extending from VHE down to radio wavelengths. In particular, the spectral energy distribution (SED) of blazars—both FSRQs and BL Lacs—exhibits two distinctive broad humps: the first, located in the IR-UV band, originates from synchrotron emission by relativistic electrons in the jet, while the second appears at gamma-ray energies. The physical origin of the high-energy hump remains under discussion. In leptonic scenarios [5–7], this component arises from inverse Compton scattering, where the same population of relativistic electrons responsible for the synchrotron emission upscatters either the synchrotron photons themselves or external photons originating from the accretion disc or surrounding gas clouds. Alternatively, hadronic models account for the high-energy emission through synchrotron radiation from ultra-relativistic protons or via photohadronic interactions, such as photomeson production [8–10]. For our purposes, it is important to specify the behavior of the magnetic field $B_{\rm jet}$ and the electron number density $n_{e,\rm jet}$ along the jet. Assuming that photons are emitted and propagate along the y-direction, the relevant component of $B_{\rm jet}$ is its toroidal part [11–13], expressed as $B_{\rm jet}(y) = B_{\rm jet,0}(y_{\rm em}/y)$, where $B_{\rm jet,0}$ denotes the field strength at the emission distance $y_{\rm em}$ from the central SMBH. Owing to the expected conical geometry of the jet, the electron number density is modeled as $n_{e,\rm jet}(y) = n_{e,\rm jet,0}(y_{\rm em}/y)^2$, with $n_{e,\rm jet,0}$ representing the value of $n_{e,\rm jet}$ at $y = y_{\rm em}$. The value of $n_{e,\rm jet,0}$ is inferred from Synchrotron Self-Compton (SSC) diagnostics applied to blazar spectra, yielding $n_{e,\rm jet,0} = 5 \times 10^4\,{\rm cm}^{-3}$ [14]. Two additional BL Lac parameters are crucial for our analysis: (i) the bulk Lorentz factor Γ, which characterizes the relativistic motion of the jet, and (ii) the initial degree of linear polarization of photons $\Pi_{L,0}$. The values of $y_{\rm em}$, $B_{\rm jet,0}$, Γ, and $\Pi_{L,0}$ depend on the specific source under consideration and on the emission model—leptonic or hadronic. The particular values used in our analysis are presented in the dedicated sections below. As a general rule, hadronic models typically require larger values of $y_{\rm em}$, $B_{\rm jet,0}$, and $\Pi_{L,0}$ compared to leptonic models, while Γ tends to be smaller.

In this review, we investigate the effects of new physics and of alternative astrophysical mechanisms on both blazar spectra and polarization. The most relevant energy bands for polarization studies are the UV-X-ray and high-energy (HE) ranges, while for spectral analyses we focus on the VHE regime. However, at VHE, another important effect must be taken into account: photons emitted at cosmological distances can interact with the IR-optical-UV radiation of the extragalactic background light (EBL; see, e.g., [15–18]) and be absorbed via the $\gamma\gamma \to e^+e^-$ process. In this review, we examine the effects of three scenarios on blazar spectra at VHE: (i) the hadron beam model as an alternative emission mechanism (see, e.g., [19–21]), and two new physics scenarios, (ii) the interaction of photons with axion-like particles (ALPs; see, e.g., [22,23]), and (iii) Lorentz invariance violation (LIV; see, e.g., [24,25]). Each of these scenarios can reduce EBL absorption and generate distinctive, potentially detectable features in the observable spectra. While all three can, therefore, lead to a photon excess at VHE, the photon–ALP scenario predicts unique spectral signatures that, if detected or excluded, can help distinguish it from the other models. Furthermore, we investigate how the photon–ALP interaction affects the polarization of blazar photons in the UV-X-ray and HE bands. The observational signatures discussed in this review are within the reach of current and upcoming instruments—both for spectral

observations, such as ASTRI Mini Array [26], CTAO [27], GAMMA-400 [28], HAWC [29], HERD [30], LHAASO [31], and TAIGA-HiSCORE [32]; and for polarimetric studies, including IXPE [33] (already operational), eXTP [34], XL-Calibur [35], NGXP [36], and XPP [37] in the X-ray band, as well as COSI [38], e-ASTROGAM [39,40], and AMEGO [41] at higher energies—making the proposed scenarios testable in the near future.

This review is structured as follows. In Section 2, we present the hadron beam scenario. Section 3 outlines the main properties and implications of the photon–ALP interaction, while Section 4 discusses Lorentz invariance violation (LIV) and its consequences. In Section 5, we analyze the impact of the three scenarios on blazar spectra, and in Section 6, we examine the effects of the photon–ALP interaction on blazar polarization. Section 7 is devoted to the discussion of the results, and we summarize our conclusions in Section 8.

Throughout this review, we employ the natural Lorentz–Heaviside (rationalized) units with $\hbar = c = k_B = 1$.

2. Hadron Beam

As discussed in the introduction, a possible explanation for the higher energy hump in blazar spectra is given by standard hadronic models, where gamma-ray photons are generated by proton-synchrotron emission or photomeson production. In the so-called hadron beam scenario, a collimated beam of ultra-relativistic hadrons accelerated in the jet is expected to escape and then to interact with extragalactic background photons producing electromagnetic cascades [19–21]. As secondary photons produced in the cascades are emitted closer to the Earth, they suffer a smaller EBL absorption resulting in a hardening of the observed blazar spectra.

However, strong crossed magnetic fields like those present in clusters and filaments can deflect the primary hadrons emitted by the source for energies $E \lesssim 10^{19}$ eV [21]. Even the extragalactic magnetic field $B_{\rm ext}$ may deflect the produced cascade depending on its strength and morphology. Unfortunately, the knowledge of the $B_{\rm ext}$ properties is still very poor, but even assuming a coherence length $\lambda_{\rm coh} = \mathcal{O}(1)$ Mpc and $B_{\rm ext} \gtrsim 10^{-15}$ G—not far above the lower observational bound [42–45]—the resulting deflection of the cosmic ray-induced cascade becomes large enough to make the hadron beam scenario inefficient at generating a TeV photon excess [46]. In fact, a sufficiently strong $B_{\rm ext}$ tends to isotropize the distribution of cosmic rays, thereby increasing the required cosmic ray luminosity to generate a significant flux of secondary photons. Moreover, the time delays introduced by the cascade process make the resulting radiation poorly compatible with sources exhibiting rapid variability [21]. This is the reason why we apply the hadron beam scenario to 1ES 0229+200 (see Section 5.2) but not to Markarian 501, which exhibits a high variability.

The main consequence of the hadron beam scenario on blazars is a spectral hardening observable at energies up to (20–30) TeV [47]. This effect becomes increasingly pronounced with the source distance: for nearby sources (redshift $z \lesssim 0.3$), a hard spectral tail is expected above ∼10 TeV, whereas for more distant ones, the tail shifts to lower energies due to enhanced EBL attenuation (see, e.g., [21]).

3. Axion-like Particles

ALPs are hypothetical particles, but they are well motivated within theories that extend the SM of particle physics, such as String Theory (e.g., [48,49]), and are currently among the best candidates for dark matter [50–53]. They constitute a generalization of the axion [54–57], the pseudo-Goldstone boson associated with the spontaneous breaking of the global Peccei–Quinn symmetry $\mathrm{U}(1)_{\rm PQ}$ introduced to solve the strong *CP* problem in quantum chromodynamics in a natural way. While the original axions interact with fermions and gluons and possess a strict relation between their mass and their coupling

with photons, ALPs primarily interact with photons (but other interactions are still possible) and the ALP mass m_a and the photon–ALP coupling $g_{a\gamma\gamma}$ are independent quantities. ALPs, denoted by a, are, therefore, very light, neutral, spin-zero pseudoscalar bosons, whose interaction with photons is described by the Lagrangian

$$\mathcal{L}_{\rm ALP} = \frac{1}{2}\,\partial^\mu a\,\partial_\mu a - \frac{1}{2}\,m_a^2\,a^2 + g_{a\gamma\gamma}\,a\,\mathbf{E}\cdot\mathbf{B}\,, \tag{1}$$

where **E** and **B** represent the electric and magnetic components of the electromagnetic tensor. Two other effects must be considered: (i) QED vacuum polarization [58–60] and (ii) photon dispersion on the CMB [61]. Several studies have obtained bounds on the ALP parameter space $(m_a, g_{a\gamma\gamma})$ [62–73], among which the most reliable constraints appear: $g_{a\gamma\gamma} < 0.66 \times 10^{-10}\,\mathrm{GeV}^{-1}$ for $m_a < 0.02\,\mathrm{eV}$ as established by the CAST Collaboration [62]; $g_{a\gamma\gamma} < 6.3 \times 10^{-13}\,\mathrm{GeV}^{-1}$ for $m_a < 10^{-12}\,\mathrm{eV}$, derived from X-ray observations of H1821+643 [70]; and $g_{a\gamma\gamma} < 5.4 \times 10^{-12}\,\mathrm{GeV}^{-1}$ for $m_a < 3 \times 10^{-7}\,\mathrm{eV}$, obtained from polarimetric studies of magnetic white dwarfs [73].

Interpreting **E** in Equation (1) as the electric field of a propagating photon and **B** as an external magnetic field, the photon–ALP interaction produces two important effects [74,75]: (i) photon–ALP oscillations, (ii) modification of the photon polarization state. In particular, ALPs have a high impact in astrophysics both on source spectra [76–86] and on photon polarization [87–97]. Currently, three independent hints point to the existence of ALPs [80,85,86], the most recent and compelling being the observation of GRB 221009A above 10 TeV, which challenges conventional physics and can be interpreted in terms of photon–ALP interaction [86].

The evaluation of the photon survival probability in the presence of photon–ALP interaction $P^{\rm ALP}_{\gamma\to\gamma}$ can be found, for instance, in the review [22]. The astrophysical spectra modified by the photon–ALP interaction are then simply given by the emitted ones multiplied by $P^{\rm ALP}_{\gamma\to\gamma}$. In particular, the photon–ALP interaction modifies the Universe transparency by partially reducing the EBL absorption: when photons oscillate into ALPs, the latter do not interact with EBL photons, thereby increasing the photon effective mean free path [79]. As a result, a photon excess is expected in blazar spectra at the energies where the EBL absorption starts to become significant [84]. Furthermore, ALP-induced spectral irregularities are also expected [84]. Instead, a detailed evaluation of the degree of linear polarization Π_L and of the polarization angle χ in the presence of photon–ALP interaction is presented, for example, in the review [23]. The photon–ALP interaction produces a variation of the initial degree of linear polarization $\Pi_{L,0}$ and energy-dependent features in the final Π_L and χ [95]. As the photon–ALP interaction is independent of the specific source state, we can study ALP-induced effects on spectra and polarization of BL Lacs in both steady and flaring states. In the following, therefore, we evaluate the ALP-induced modifications to the spectra of both Markarian 501 and 1ES 0229+200 (see Sections 5.1 and 5.2) and to the polarization of OJ 287 (see Section 6).

4. Lorentz Invariance Violation

Achieving a unified theory of all fundamental interactions at the quantum level requires the quantization of gravity. Since gravity is a theory of dynamical spacetime, it produces its own fluctuations and the spacetime assumes a foam-like structure with a continuously changing metric and topology [98–101]. Studies have shown that such a spacetime foam behaves analogously to a quantum thermal bath, resulting in loss of coherence [102,103]. This dynamical vacuum affects the particle propagation, giving rise to a LIV at a scale $E_{\rm LIV}$ close to the Planck mass $M_P \equiv (\hbar c/G)^{1/2} \simeq 1.22 \times 10^{19}\,\mathrm{GeV}$. LIV exhibits a rich phenomenology, leading to modifications of standard physical interactions and permitting processes that are otherwise forbidden within conventional physics, such as

the vacuum Cherenkov effect, photon decay, photon splitting, and changes in the threshold of reactions [104].

In particular, LIV alters the standard photon dispersion relation by introducing additional energy-dependent terms of the form $E^{n+2}/E^n_{\rm LIV}$, with E representing the photon energy and n the order of the term (see, e.g., [24]). Considering the leading-order correction with $n = 1$, the dispersion relation for photons becomes

$$E^2 - p^2 = \pm \frac{E^3}{E_{\rm LIV}}\,, \tag{2}$$

with p denoting the photon momentum. The sign on the right-hand side of Equation (2) defines the so-called superluminal $(+)$ or subluminal $(-)$ case. While the superluminal case induces photon decay at TeV energies testable for galactic sources [105], we are interested here in the subluminal one, which produces a modification in the threshold of the process $\gamma\gamma \to e^+e^-$. Equation (2) shows that the LIV effects become increasingly significant with rising photon energy. As a consequence, the EBL absorption turns out to be strongly reduced for $E \gtrsim \mathcal{O}(10)$ TeV depending on the value assumed by $E_{\rm LIV}$, which produces an observable hardening and detectable signatures in the blazar spectra [25]. While many bounds on $E_{\rm LIV}$ exist in the literature (see, e.g., [106–111]), the recent detection of a photon from GRB 221009A with energy up to 300 TeV—incompatible with standard physics—has been interpreted as a potential signature of LIV [112].

The photon survival probability in the presence of LIV, denoted as $P^{\rm LIV}_{\gamma\to\gamma}$, is evaluated, for example, in [25]. The corresponding modification of the astrophysical spectra due to LIV effects is then obtained simply by multiplying the emitted spectrum by $P^{\rm LIV}_{\gamma\to\gamma}$. In particular, the LIV scenario induces a strong spectral hardening for $E \gtrsim \mathcal{O}(10)$ TeV: therefore, the best candidates to test these features are high-frequency peaked BL Lacs (HBLs) and extreme HBLs (EHBLs), as they can be observable up to few TeV [25,113]. Since the LIV effects are independent of the particular properties or state of the considered BL Lac, we can apply the LIV scenario to both steady- and flaring-state BL Lacs. Therefore, we discuss the LIV impact on the spectra of both Markarian 501 and 1ES 0229+200 (see Sections 5.1 and 5.2).

5. Spectral Analysis

Following the approach presented in [114], we now examine the effects on blazar spectra at VHE of the three scenarios introduced above: (i) the hadron beam model, (ii) photon–ALP interaction, and (iii) LIV. We highlight both their similarities and distinctive features that may help distinguish between them. For this purpose, we focus on two particularly promising BL Lacs: Markarian 501 and 1ES 0229+200. As benchmark values, we adopt $m_a = 10^{-10}$ eV and $g_{a\gamma\gamma} = 10^{-11}\,{\rm GeV}^{-1}$ for the ALP scenario, and $E_{\rm LIV} = 10^{20}\,{\rm GeV}$ for the LIV case. For the EBL, we employ the model described in [17]. Throughout this section, E denotes the photon energy as measured on Earth.

5.1. Markarian 501

Markarian 501 is a bright high-frequency peaked BL Lac (HBL) located at a redshift $z = 0.034$. Its active states, whose most impressive example is represented by the HEGRA observations reaching energies above 10 TeV with a hard spectrum [115], are considered extremely promising for the study of possible new physics signals [25]. Due to the high variability of Markarian 501, the hadron beam scenario is not applicable to this source, so that, as reported in Figure 1, we consider only the effects induced by the photon–ALP interaction and by LIV. Concerning the emission mechanism, we assume a leptonic model with $y_{\rm em} = 3 \times 10^{16}$ cm, $B_{\rm jet,0} = 0.5\,{\rm G}$, and $\Gamma = 15$ [82]. Moreover, to describe the intrinsic

spectrum, we adopt an exponentially truncated power law with energy index $\alpha_1 = 1$ and cutoff energy $E_{\rm cut} = 20\,\text{TeV}$ (for more details see [114]).

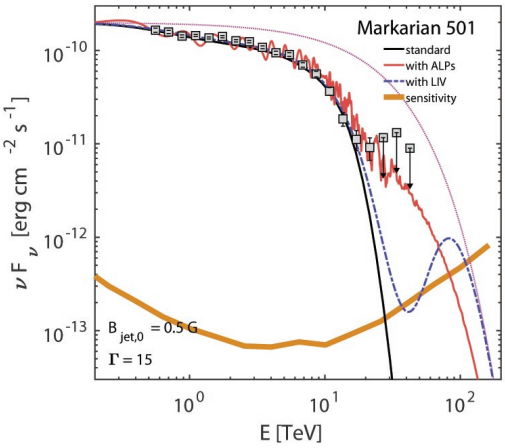

Figure 1. Spectrum of Markarian 501 versus E in the band (0.2–200) TeV within conventional physics (solid black line), photon–ALP interaction scenario (solid red line), and LIV model (dot-dashed blue line). The dotted purple line is the intrinsic exponentially truncated power law spectrum, and the solid orange line is the CTAO sensitivity with 50 h of observation. We assume $g_{a\gamma\gamma} = 10^{-11}\,\text{GeV}^{-1}$ and $m_a = 10^{-10}\,\text{eV}$ for the ALP scenario and $E_{\rm LIV} = 10^{20}\,\text{GeV}$ for the LIV case. We take $B_{\rm jet,0} = 0.5\,\text{G}$ and $\Gamma = 15$. The grey squares are the observational data detected by HEGRA [115] (credit: [114]).

As discussed in [114], Figure 1 shows that the photon–ALP interaction produces two effects: (i) observable spectral irregularities at lower energies ($E \lesssim 5\,\text{TeV}$); (ii) a photon excess with respect to conventional physics for energies above ∼10 TeV (see also [84,114]). Instead, LIV leads to a spectral hardening above approximately ∼20 TeV (see also [114]), which is similar to the effect produced by the photon–ALP interaction. However, unlike the ALP scenario, LIV additionally predicts a distinctive minimum in the spectrum near 40 TeV, followed by a peak around 100 TeV.

A photon excess above ∼10 TeV is unexpected within conventional physics due to EBL absorption; therefore, it could indicate new physics, potentially due to ALPs or LIV, although such a signal alone would not distinguish between the two scenarios. However, the possible detection of spectral irregularities would incontrovertibly indicate the ALP scenario, as such a feature is not predicted by LIV. All the ALP- and LIV-induced signatures reported in Figure 1 are expected to be observable by CTAO for a 50 h exposure [27,114].

5.2. 1ES 0229+200

1ES 0229+200 is the archetype of extreme high-frequency peaked BL Lacs (EHBLs), with a hard spectrum observed beyond 10 TeV [116], despite its relatively high redshift $z = 0.1396$, where the EBL absorption at TeV energies is strong (see, e.g., [17]). Moreover, EHBLs show an untypical low variability with respect to other BL Lacs [117], which allows us to apply to 1ES 0229+200 not only the photon–ALP interaction and LIV models but also the hadron beam scenario, as shown in Figure 2.

As the EHBL behavior is not yet completely understood, we consider both a leptonic emission model with $y_{\rm em} = 3 \times 10^{16}\,\text{cm}$, $B_{\rm jet,0} = 2\,\text{mG}$, and $\Gamma = 50$ [118] and a hadronic one with $y_{\rm em} = 3 \times 10^{16}\,\text{cm}$, $B_{\rm jet,0} = 0.5\,\text{G}$, and $\Gamma = 15$ [119] in the left and right panels of Figure 2, respectively. Furthermore, we adopt two different descriptions of the intrinsic spectrum: (i) an exponentially truncated power law with energy index $\alpha_1 = 0.4$ and cutoff energy $E_{\rm cut} = 15\,\text{TeV}$ in the upper panels of Figure 2; (ii) a broken power law with different parameters for the photon–ALP conversion model and the LIV scenario in the lower panels

of Figure 2, by taking energy indices $\alpha_1^{\rm ALP} = 0.6$ and $\alpha_1^{\rm LIV} = 0.4$, high-energy indices $\alpha_2^{\rm ALP} = 2.2$ and $\alpha_2^{\rm LIV} = 2$, and break energy $E_b^{\rm ALP} = E_b^{\rm LIV} = 10\,\text{TeV}$.

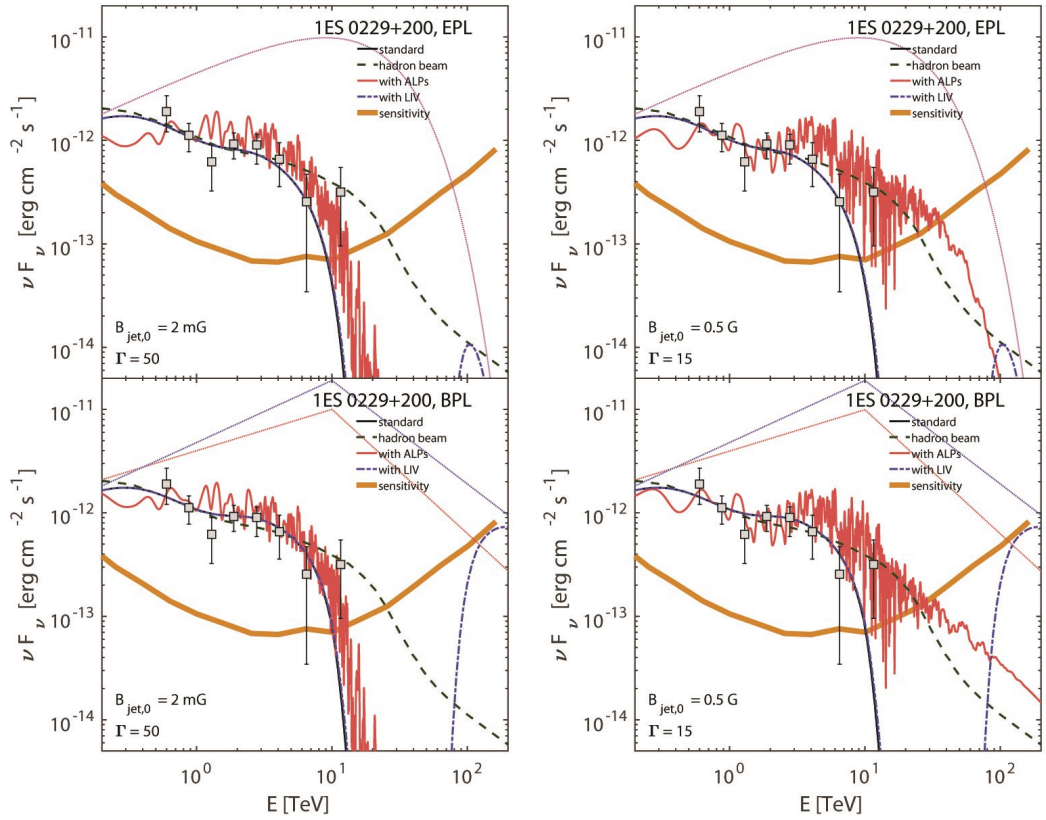

Figure 2. Same as Figure 1 but for 1ES 0229+200. Moreover, the dashed green line describes the hadron beam scenario. In the *upper panels*, we assume an intrinsic exponentially truncated power law (EPL) spectrum (for both the photon–ALP interaction and the LIV scenario) corresponding to the dotted purple line, while in the *lower panels*, we consider an intrinsic broken power law (BPL) spectrum [two different models are assumed for the photon–ALP interaction scenario (dotted red line) and the LIV one (dotted blue line)]. We assume $g_{a\gamma\gamma} = 10^{-11}\,\text{GeV}^{-1}$ and $m_a = 10^{-10}\,\text{eV}$ for the ALP scenario and $E_{\rm LIV} = 10^{20}\,\text{GeV}$ for the LIV case. In the *left panels*, we consider the leptonic emission model with $B_{\rm jet,0} = 2\,\text{mG}$ and $\Gamma = 50$, while in the *right panels* the hadronic one with $B_{\rm jet,0} = 0.5\,\text{G}$ and $\Gamma = 15$. The grey squares represent the observational data from HESS [116] (credit: [114]).

Figure 2 shows that the hadron beam scenario remains unaffected by both the emission mechanism (leptonic or hadronic) and the assumed intrinsic spectrum. In contrast, the LIV case is sensitive to the choice of the intrinsic spectral model, while the photon–ALP interaction scenario depends on both the intrinsic spectrum and the emission mechanism. Therefore, in all the panels of Figure 2, the hadron beam scenario yields a hard tail above $\sim$10 TeV extending smoothly beyond 100 TeV, as reported in [114]. Furthermore, the photon–ALP interaction scenario generates two effects: (i) observable energy-dependent spectral irregularities at lower energies ($E \lesssim 5\,\text{TeV}$); (ii) a photon excess above $\sim$10 TeV (see also [84,114]). While the presence of the spectral irregularities is independent of the intrinsic spectrum and of the emission mechanism, the photon excess above $\sim$10 TeV is more evident in the case of the hadronic model due to the higher value of $B_{\rm jet,0}$, which is responsible for a more efficient photon–ALP conversion inside the jet. The broken power law intrinsic spectrum mildly increases the latter effect and only at the highest considered energies. The LIV scenario does not predict substantial effects around $\sim$10 TeV but produces a peculiar peak around $\sim$100 TeV, which is, however, detectable only in the case of an intrinsic broken power law spectrum when compared to the predicted CTAO sensitivity [27,114].

The possible detection of a harder spectra above ∼10 TeV with respect to standard expectations could be explained either by the hadron beam or by the photon–ALP interaction scenario provided that the emission is of hadronic origin. However, a definitive way to discriminate between these two possibilities lies in the potential observation of spectral irregularities, which are peculiar of the photon–ALP interaction scenario. On the other hand, a spectral feature observed near ∼100 TeV would point exclusively toward a LIV scenario, since only LIV predicts such a high-energy signature. The above-described features produced by the three considered scenarios are expected to be observable by CTAO for a 50 h exposure [27,114].

6. Polarization Analysis

As detailed in [95,97], we investigate the impact of the photon–ALP interaction on the polarization of photons from blazars in the UV-X-ray and HE bands, focusing specifically on OJ 287. This interaction affects both the final degree of linear polarization Π_L, and the polarization angle χ. Since the exact configuration of the encountered magnetic fields—particularly their orientations—is uncertain and can strongly influence Π_L, we perform multiple simulations varying the magnetic field properties during the photon–ALP beam propagation. This produces a distribution of Π_L values, from which we derive a probability density function f_Π, highlighting the most probable polarization outcomes and helping assess the robustness of our results.

It is important to note that real polarimeters have limited spatial resolution and cannot distinguish photons emitted from different regions across the jet transverse section, instead collecting all photons together. Although this could, in principle, dilute ALP-induced polarization signatures, the analyses in [95,97] demonstrate that this effect is negligible in realistic observational scenarios. To be conservative, we assume a photon–ALP beam propagation length of 1 pc inside the jet (see [95,97] for details on how the polarimeter limitations are incorporated). In this section, E_0 stands for the photon energy as observed from Earth.

OJ 287

OJ 287 is a low-frequency peaked BL Lac (LBL) lying at redshift $z = 0.3056$. Thanks to its strong emission in both the X-ray and HE bands, OJ 287 is considered a promising candidate for polarimetric observations across these energy ranges [120]. Regarding the emission mechanism we assume the typical values for the LBL parameters: $y_{\rm em} = 3 \times 10^{16}$ cm, $B_{\rm jet,0} = 1$ G, and $\Gamma = 10$ for the leptonic model and $y_{\rm em} = 10^{17}$ cm, $B_{\rm jet,0} = 20$ G, and $\Gamma = 15$ [121] for the hadronic model. The profile of the initial degree of linear polarization $\Pi_{L,0}$ for both the leptonic and hadronic cases is derived in [120] and reported in Figures 3–5 as a reference, where it is represented by the dashed gray line. We concentrate on two different energy bands: (i) UV-X-ray band in Figure 3, where we assume $g_{a\gamma\gamma} = 0.5 \times 10^{-11}\,{\rm GeV}^{-1}$ and $m_a \lesssim 10^{-14}$ eV; (ii) HE band, with the same parameter values in Figure 4, and $m_a = 10^{-10}$ eV in Figure 5.

In particular, in the UV-X-ray band $(4 \times 10^{-2} - 10^2)$ keV, we show $P_{\gamma\to\gamma}$, Π_L, and χ in the top subfigure of Figure 3 and the corresponding behavior of f_Π for the benchmark energies: (i) $E_0 = 1$ keV and (ii) $E_0 = 10$ keV in the bottom subfigure of Figure 3. Results within the leptonic emission model are reported in the left panels of Figure 3, while those within the hadronic one in the right panels of Figure 3. We recall that in the present situation, we assume the ALP parameters: $g_{a\gamma\gamma} = 0.5 \times 10^{-11}\,{\rm GeV}^{-1}$, $m_a \lesssim 10^{-14}$ eV. As shown by the top subfigure of Figure 3, the photon–ALP beam propagates in the weak mixing regime in the UV-X-ray band since the plasma effect plays a non-negligible role compared to the photon–ALP mixing term particularly within the jet of OJ 287. As a consequence, $P_{\gamma\to\gamma}$, Π_L and χ in the top subfigure of Figure 3 show an energy-dependent behavior for

a few decades, as a result of the strong variation of $B_{\rm jet}$ and $n_{e,\rm jet}$ with the distance (for details see also [95,97]). The binned data in the top subfigure of Figure 3 concerning the final Π_L show that not only is Π_L strongly modified with respect to the initial $\Pi_{L,0}$ both in the leptonic and hadronic cases, but also that observatories such as IXPE [33], eXTP [34], XL-Calibur [35], NGXP [36], and XPP [37] may detect the polarization features induced by the photon–ALP interaction for $E_0 \gtrsim 0.5\,\text{keV}$. Furthermore, we can observe that in the hadronic model, the energy-dependent variation of Π_L and χ is more pronounced than in the leptonic scenario, owing to the higher value of $B_{\rm jet,0}$ and the larger spatial extent of the jet region.

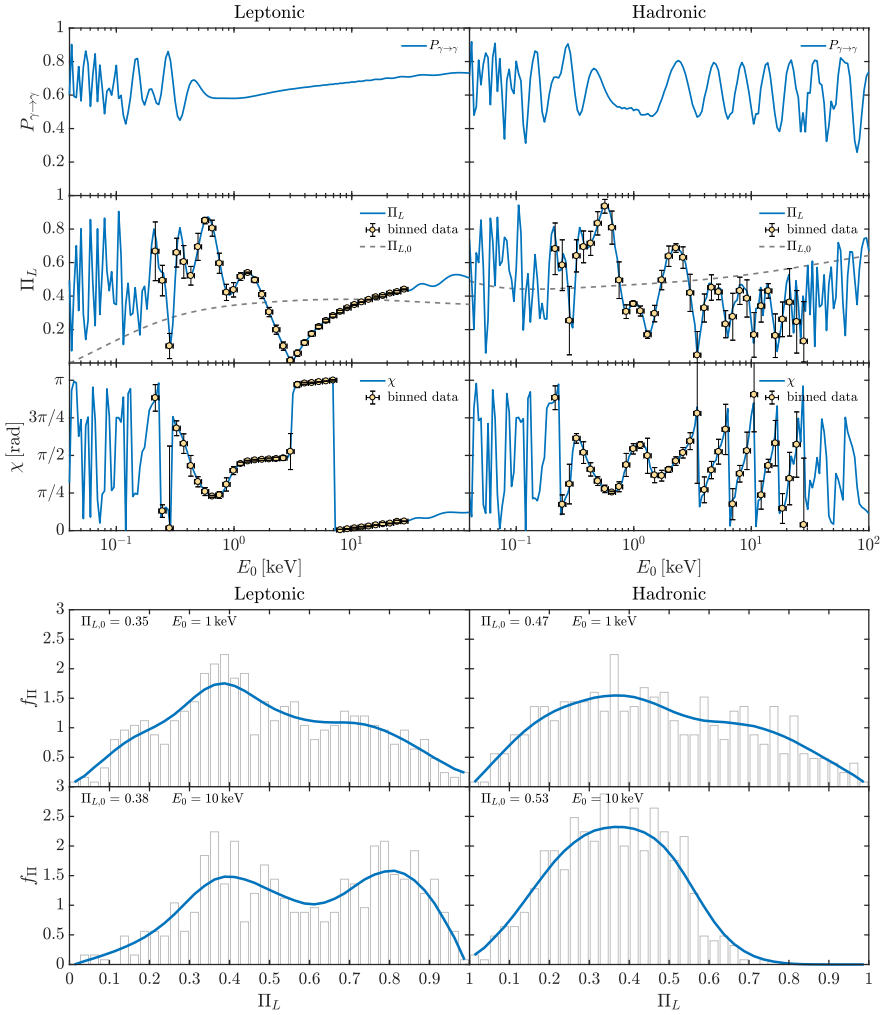

Figure 3. The photon survival probability $P_{\gamma\to\gamma}$ (*upper panels*), the final degree of linear polarization Π_L (*central panels*), and the final polarization angle χ (*lower panels*) for OJ 287 in the energy range $(4\times10^{-2} - 10^2)$ keV are shown in the *top subfigure*, where the initial degree of linear polarization $\Pi_{L,0}$ is also reported (dashed gray line). The probability density functions f_Π obtained by interpolating the plotted histogram for multiple realizations of Π_L at 1 keV (*upper panels*) and 10 keV (*lower panels*) are shown in the *bottom subfigure*. The leptonic and hadronic emission mechanisms are considered in the *left* and *right columns*, respectively. We take $g_{a\gamma\gamma} = 0.5\times10^{-11}\,\text{GeV}^{-1}$, $m_a \lesssim 10^{-14}\,\text{eV}$ (credit: [97]).

The bottom subfigure of Figure 3 reports the behavior of f_Π, showing a broadening of the final Π_L if compared to the initial $\Pi_{L,0}$. Around $E_0 = 1\,\text{keV}$, the most probable final value of Π_L remains quite consistent with the initial polarization degree $\Pi_{L,0}$, while around $E_0 = 10\,\text{keV}$ and in the case of the leptonic model, the most probable outcome exceeds $\Pi_L \gtrsim 0.8$, which represents a value that is difficult to reconcile with predictions from conventional physics (see [97] for more details). Therefore, the latter case represents

an interesting candidate for a case study to search for ALP-induced polarization features in blazars.

Instead, in the HE band $(10^{-1} - 5 \times 10^2)$ MeV, we start by considering the case $g_{a\gamma\gamma} = 0.5 \times 10^{-11}\,\mathrm{GeV}^{-1}$, $m_a \lesssim 10^{-14}$ eV. Correspondingly, the behavior of $P_{\gamma\to\gamma}$, Π_L and χ is shown in the top subfigure of Figure 4 and the derived f_Π for the benchmark energies: (i) $E_0 = 300$ keV and (ii) $E_0 = 3$ MeV in the bottom subfigure of Figure 4. The results obtained under the leptonic emission model are presented in the left panels of Figure 4, whereas those derived from the hadronic emission model are shown in the right panels. The top subfigure of Figure 4 shows that the photon–ALP beam propagates in the strong mixing regime throughout almost the entire considered energy band, as the photon–ALP mixing term dominates over all other effects producing a behavior of $P_{\gamma\to\gamma}$, Π_L, and χ, which is energy independent for $E_0 \gtrsim (0.5 - 1)$ MeV. We further observe that the final Π_L, is significantly altered compared to its initial value $\Pi_{L,0}$, but no appreciable differences emerge between the leptonic and hadronic emission models. The binned data in the top subfigure of Figure 4 exhibit reduced uncertainties with respect to those in the UV-X-ray band, primarily due to the fact that the photon–ALP system remains in the strong mixing regime across the relevant energy range. As a result, OJ 287 turns out to be a particularly promising observational target for future polarimetric missions, such as COSI [38], e-ASTROGAM [39,40], and AMEGO [41].

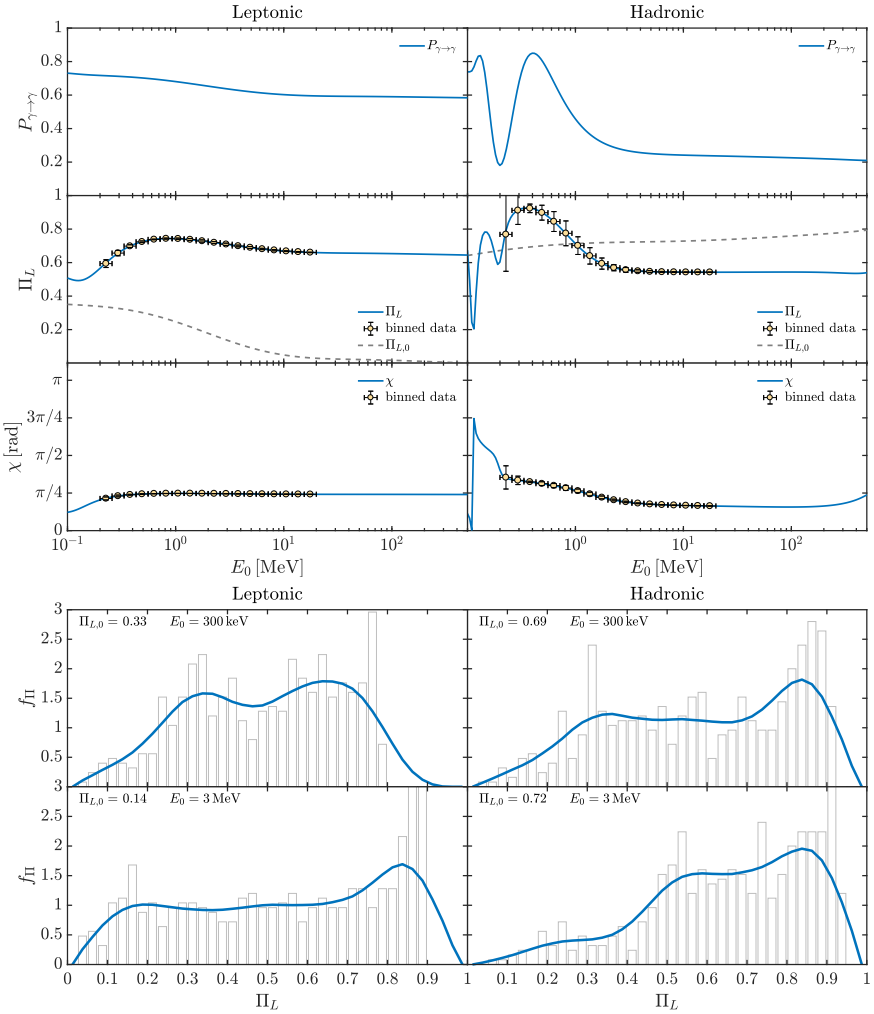

Figure 4. Same as Figure 3 but for the energy range $(10^{-1} - 5 \times 10^2)$ MeV, as shown in the *top subfigure* and for f_Π evaluated at 300 keV (*upper panels*) and 3 MeV (*lower panels*), as reported in the *bottom subfigure*. We take $g_{a\gamma\gamma} = 0.5 \times 10^{-11}\,\mathrm{GeV}^{-1}$, $m_a \lesssim 10^{-14}$ eV (credit: [97]).

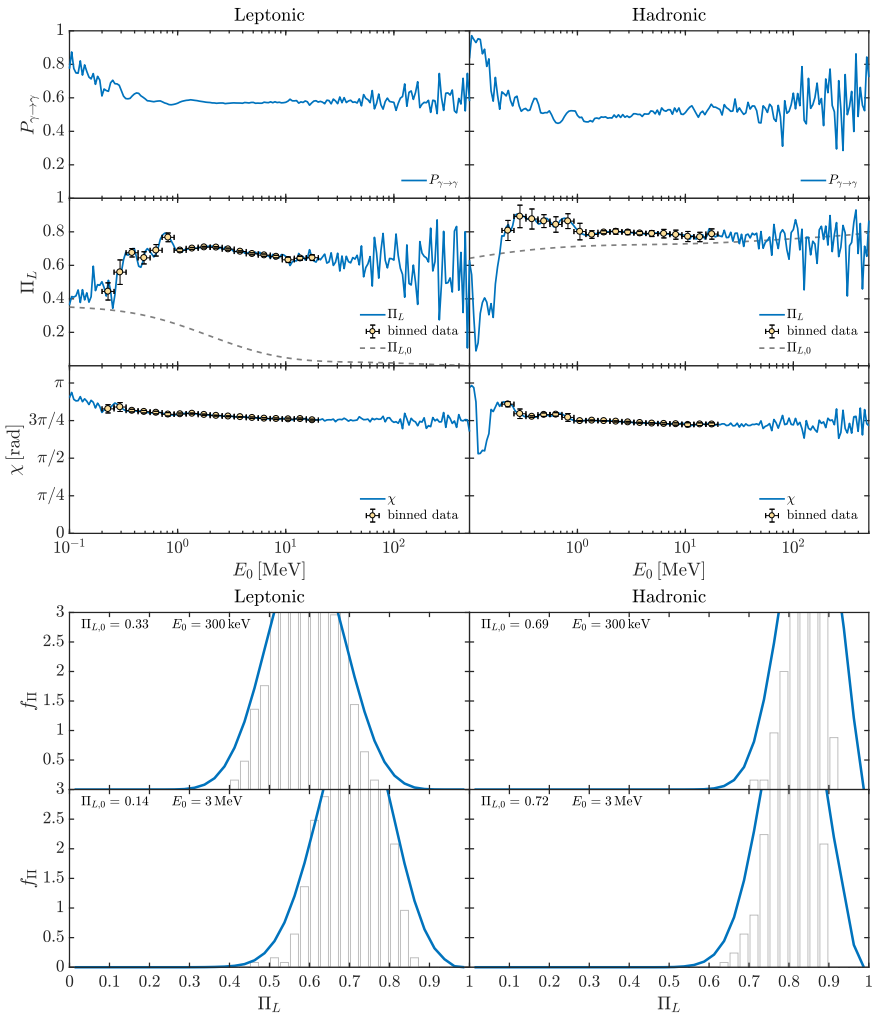

Figure 5. Same as Figure 4. We take $g_{a\gamma\gamma} = 0.5 \times 10^{-11}\,\mathrm{GeV}^{-1}$, $m_a = 10^{-10}\,\mathrm{eV}$ (credit: [97]).

The behavior of f_Π reported in the bottom subfigure of Figure 4 indicates that the most probable final value of Π_L exceeds the initial $\Pi_{L,0}$ with a marked broadening. The energy range around $E_0 = 3\,\mathrm{MeV}$ emerges as particularly favorable for probing ALP-induced effects on photon polarization, as the most probable value of Π_L reaches $\Pi_L \gtrsim 0.8$, which is significantly higher than standard physics expectations.

Still, in the HE band $(10^{-1} - 5 \times 10^2)\,\mathrm{MeV}$ but taking the ALP parameters $g_{a\gamma\gamma} = 0.5 \times 10^{-11}\,\mathrm{GeV}^{-1}$, $m_a = 10^{-10}\,\mathrm{eV}$, we report the behavior of $P_{\gamma\to\gamma}$, Π_L and χ in the top subfigure of Figure 5 and the associated f_Π for the benchmark energies: (i) $E_0 = 300\,\mathrm{keV}$, (ii) $E_0 = 3\,\mathrm{MeV}$ in the bottom subfigure of Figure 5. The left panels of Figure 5 display the results obtained within the leptonic emission model, while the right panels report the findings within the hadronic one. As shown by the top subfigure of Figure 5, the photon–ALP system propagates in the weak mixing regime, as the effect of the higher ALP mass term ($m_a = 10^{-10}\,\mathrm{eV}$ with respect to the previously considered $m_a \lesssim 10^{-14}\,\mathrm{eV}$) cannot be neglected in comparison with the photon–ALP mixing term. Consequently, $P_{\gamma\to\gamma}$, Π_L and χ turn out to be energy dependent in all the examined band with a substantial modification of the final Π_L with respect to the initial $\Pi_{L,0}$ especially in the leptonic case. As previously noted in the X-ray band for $g_{a\gamma\gamma} = 0.5 \times 10^{-11}\,\mathrm{GeV}^{-1}$ and $m_a \lesssim 10^{-14}\,\mathrm{eV}$, the extended energy range over which the photon–ALP system remains in the weak mixing regime arises from the significant spatial variation of B_{jet} and $n_{e,\mathrm{jet}}$ (see also [95,97] for further details). The binned data presented in the top subfigure of Figure 5 suggest that future polarimetric missions, such as COSI [38], e-ASTROGAM [39,40], and

AMEGO [41], could be sensitive to ALP-induced modifications of Π_L for $E_0 \gtrsim 0.2\,\mathrm{MeV}$, under both leptonic and hadronic emission scenarios.

The bottom subfigure of Figure 5 reporting the behavior of f_Π shows a broadening of the final Π_L compared to the initial $\Pi_{L,0}$. The most probable value of the final Π_L is significantly larger than the initial one $\Pi_{L,0}$ within the leptonic model, making it an interesting case study especially for $E_0 \gtrsim 3\,\mathrm{MeV}$. Instead, within the hadronic model, the modification of Π_L with respect to $\Pi_{L,0}$ is less marked, making it a less compelling object of investigation.

7. Discussion and Future Perspectives

In Section 5, we have demonstrated that blazar spectra at VHE can exhibit imprints of the three scenarios beyond the standard paradigm, discussed in this review (see [114] for further details): the hadron beam model, the photon–ALP interaction, and LIV. Our analysis has focused on two representative BL Lacs: Markarian 501 and 1ES 0229+200. In particular, when the hadron beam model is applicable—notably for steady sources such as 1ES 0229+200—both the hadron beam and the photon–ALP interaction scenarios predict a photon excess at energies $E \gtrsim 10\,\mathrm{TeV}$, where the EBL absorption is significant. However, only the photon–ALP interaction induces distinctive energy-dependent oscillatory features in the range $0.5\,\mathrm{TeV} \lesssim E \lesssim 5\,\mathrm{TeV}$. In contrast, the LIV scenario leads to a photon excess at much higher energies, around 100 TeV. As a result, the three scenarios may be distinguishable based on the observed spectral features and energy band. We have also shown that, given a reasonable exposure time, CTAO [27] is expected to be able to detect the spectral signatures predicted by these scenarios, provided that they are realized in nature. For instance, a possible detection by CTAO [27] of photon excess around 100 TeV would strongly favor LIV. Conversely, an excess at $E \gtrsim 10\,\mathrm{TeV}$ could arise from either the hadron beam or the photon–ALP interaction scenario. However, the presence or absence of the mentioned spectral irregularities—likely resolvable with CTAO expected energy resolution [27]—would provide a way to discriminate between them. Additionally, the ASTRI Mini Array [26] may also detect significant deviations from standard predictions related to photon excesses, provided that the exposure time is sufficiently long. Other facilities, such as GAMMA-400 [28], HAWC [29], HERD [30], LHAASO [31], and TAIGA-HiSCORE [32], also have the potential to detect the effects of the three considered scenarios on blazar spectra, possibly providing evidence or placing new constraints on their properties.

Similarly, in Section 6, we have demonstrated that the polarization of photons emitted from blazars may carry distinctive signatures of the photon–ALP interaction, in both the UV-X-ray and HE bands (see [95,97] for more details). We have focused on the representative BL Lac OJ 287 and found that the photon–ALP interaction can significantly alter the final degree of linear polarization Π_L with respect to the initial one $\Pi_{L,0}$. In particular, when Π_L reaches very high values (e.g., $\Pi_L \gtrsim 0.8$), blazars become very promising candidates for detecting ALP-induced polarization effects. In such potential cases, even hadronic emission models struggle to explain the observations within the framework of standard physics [97]. A potential detection of $\Pi_L \gtrsim 0.8$ by observatories such as IXPE [33] in the X-ray band would therefore provide strong evidence in support of the ALP existence. Prospectively, future or already-approved missions like eXTP [34], XL-Calibur [35], NGXP [36], and XPP [37] in the UV-X-ray range, as well as COSI [38], e-ASTROGAM [39,40], and AMEGO [41] in the HE band, are expected to offer enhanced sensitivity. These instruments could either strengthen evidence for ALPs or further constrain their parameter space. On the contrary, lower Π_L values remain compatible with standard physics under hadronic emission models. However, recent IXPE observations [122–130] challenge scenarios with initially high $\Pi_{L,0}$, and new theoretical models suggest that the turbulent structure of the jet magnetic field

$B_{\rm jet}$ may naturally reduce $\Pi_{L,0}$ [131]. While the photon–ALP interaction can either increase or decrease the final polarization, LIV tends only to suppress Π_L [132]. Additionally, LIV can induce an energy-dependent rotation of the linear polarization plane for photons from blazars—a vacuum birefringence effect—observable in both the optical-X-ray and HE bands [133–135]. Such signatures may be exploited to constrain or even detect LIV, especially with the next-generation polarimetric missions mentioned above.

In this review, we have adopted benchmark values for key BL Lac properties, such as $y_{\rm em}$ and $B_{\rm jet,0}$. A full exploration of the BL Lac parameter space lies beyond our scope; however, as shown in [82], variations in $y_{\rm em}$ and $B_{\rm jet,0}$ only mildly affect the photon–ALP interaction scenario. In particular, larger values of these parameters lead to stronger photon–ALP conversion in the jet, potentially resulting in tighter constraints on the ALP parameter space $(m_a, g_{a\gamma\gamma})$ from both spectral and polarization studies.

8. Conclusions

In this review, we have presented blazars as privileged astrophysical laboratories for probing alternative emission mechanisms and fundamental physics. In particular, we have explored the impact on blazars of three scenarios beyond the standard paradigm: (i) the hadron beam model, (ii) the photon–ALP interaction, and (iii) LIV.

We have analyzed how these scenarios affect blazar spectra, identifying Markarian 501 and 1ES 0229+200 as particularly promising sources. We have also shown that, although these scenarios may produce a similar photon excess at VHE, we can discriminate among them by searching for ALP-induced spectral irregularities (see also [114]). These investigations are timely, as current and upcoming facilities—such as ASTRI Mini Array [26], CTAO [27], GAMMA-400 [28], HAWC [29], HERD [30], LHAASO [31], and TAIGA-HiSCORE [32]—have the potential to detect deviations from standard predictions.

We have also examined the effects of the photon–ALP interaction on the polarization of photons from blazars, focusing in particular on the BL Lac OJ 287. The induced modifications to the final degree of linear polarization can be significant (see also [95,97]), and potentially detectable by missions such as IXPE [33], eXTP [34], XL-Calibur [35], NGXP [36], and XPP [37] in the X-ray band, as well as COSI [38], e-ASTROGAM [39,40], and AMEGO [41] in the HE range. In addition to blazars, galaxy clusters also represent very promising targets to investigate ALP-induced effects on photon polarization with the aforementioned observatories. Indeed, while their diffuse emission is expected to be entirely unpolarized in the X-ray and HE bands under standard physics, the photon–ALP interaction can induce a detectable level of polarization [95,96].

Both spectral and polarimetric studies have the potential to find hints at the above-mentioned three scenarios or to constrain their parameter space further. Therefore, a promising future lies ahead for fundamental physics, with blazars serving as natural laboratories to test scenarios beyond the standard paradigm. This approach may help us to drive theoretical research in a well-defined direction.

Funding: The work of the author is supported by a contribution from Grant No. ASI-INAF 2023-17-HH.0 and by the INAF Mini Grant 'High-energy astrophysics and axion-like particles', PI: Giorgio Galanti.

Data Availability Statement: Data used in this paper can be requested from the authors of the quoted papers.

Acknowledgments: The author thanks all collaborators in this field, and especially Enrico Costa, Alessandro De Angelis, Marco Roncadelli, and Fabrizio Tavecchio.

Conflicts of Interest: The author declares no conflicts of interest.

References

1. Urry, C.M.; Padovani, P. Unified schemes for radio-loud active galactic nuclei. *Pub. Astron. Soc. Pac.* **1995**, *107*, 803. [CrossRef]
2. Galanti, G.; Landoni, M.; Tavecchio, F.; Covino, S. Probing the absorption of gamma-rays by IR radiation from the dusty torus in FSRQs with the Cherenkov telescope array. *Mon. Not. Astron. R. Soc.* **2020**, *495*, 3463. [CrossRef]
3. Ghisellini, G.; Maraschi, L.; Tavecchio, F. The *Fermi* blazars' divide. *Mon. Not. Astron. R. Soc.* **2009**, *396*, L105. [CrossRef]
4. Righi, C.; Tavecchio, F.; Inoue, S. Neutrino emission from BL Lac objects: The role of radiatively inefficient accretion flows. *Mon. Not. Astron. R. Soc.* **2019**, *483*, L127. [CrossRef]
5. Maraschi, L.; Ghisellini, G.; Celotti, A. A jet model for the gamma-ray emitting blazar 3C 279. *Astrophys. J.* **1992**, *397*, L5–L9. [CrossRef]
6. Sikora, M.; Begelman, M.G.; Rees, M.J. Comptonization of diffuse ambient radiation by a relativistic jet: The source of gamma rays from blazars? *Astrophys. J.* **1994**, *421*, 153–162. [CrossRef]
7. Bloom, S.D.; Marscher, A.P. An analysis of the synchrotron self-compton model for the multi–wave band spectra of blazars. *Astrophys. J.* **1996**, *461*, 657. [CrossRef]
8. Mannheim, K. The proton blazar. *Astron. Astrophys.* **1993**, *269*, 67–76.
9. Mannheim, K. TeV gamma-rays from proton blazars. *Space Sci. Rev.* **1996**, *75*, 331–340. [CrossRef]
10. Mücke, A.; Protheroe, R.J.; Engel, R.; Rachen, J.P.; Stanev, T. BL Lac objects in the synchrotron proton blazar model. *Astropart. Phys.* **2003**, *18*, 593. [CrossRef]
11. Begelman, M.C.; Blandford, R.D.; Rees, M.J. Theory of extragalactic radio sources. *Rev. Mod. Phys.* **1984**, *56*, 255–351. [CrossRef]
12. Ghisellini, G.; Tavecchio, F. Canonical high-power blazars. *Mon. Not. Astron. R. Soc.* **2009**, *397*, 985–1002. [CrossRef]
13. Pudritz, R.E.; Hardcastle, M.J.; Gabuzda, D.C. Magnetic Fields in Astrophysical Jets: From Launch to Termination. *Space Sci. Rev.* **2012**, *169*, 27–72. [CrossRef]
14. Tavecchio, F.; Ghisellini, G.; Ghirlanda, G.; Foschini, L.; Maraschi, L. TeV BL Lac objects at the dawn of the *Fermi* era. *Mon. Not. Astron. R. Soc.* **2010**, *401*, 1570–1586. [CrossRef]
15. De Angelis, A.; Galanti, G.; Roncadelli, M. Transparency of the Universe to gamma rays. *Mon. Not. Astron. R. Soc.* **2013**, *432*, 3245. [CrossRef]
16. Dwek, E.; Krennrich, F. The extragalactic background light and the gamma-ray opacity of the universe. *Astropart. Phys.* **2013**, *43*, 112. [CrossRef]
17. Franceschini, A.; Rodighiero, G. The extragalactic background light revisited and the cosmic photon-photon opacity. *Astron. Astrophys.* **2017**, *603*, A34. [CrossRef]
18. Galanti, G.; Piccinini, F.; Roncadelli, M.; Tavecchio, F. Estimating $\gamma\gamma$ absorption for ultrahigh-energy photons with lepton and hadron production. *Phys. Rev. D* **2020**, *102*, 123004. [CrossRef]
19. Essey, W.; Kusenko, A. A new interpretation of the gamma-ray observations of distant active galactic nuclei. *Astropart. Phys.* **2010**, *33*, 81. [CrossRef]
20. Essey, W.; Kalashev, O.; Kusenko, A.; Beacom, J.F. Role of Line-of-sight Cosmic-ray Interactions in Forming the Spectra of Distant Blazars in TeV Gamma Rays and High-energy Neutrinos. *Astrophys. J.* **2011**, *731*, 51. [CrossRef]
21. Murase, K.; Dermer, C.D.; Takami, H.; Migliori, G. Blazars as Ultra-high-energy Cosmic-ray Sources: Implications for TeV Gamma-Ray Observations. *Astrophys. J.* **2012**, *749*, 63. [CrossRef]
22. Galanti, G.; Roncadelli, M. Axion-like Particles Implications for High-Energy Astrophysics. *Universe* **2022**, *8*, 253. [CrossRef]
23. Galanti, G. Axion-like Particle Effects on Photon Polarization in High-Energy Astrophysics. *Universe* **2024**, *10*, 312. [CrossRef]
24. Kifune, T. Invariance Violation Extends the Cosmic-Ray Horizon? *Astrophys. J.* **1999**, *518*, L21. [CrossRef]
25. Tavecchio, F.; Bonnoli, G. On the detectability of Lorentz invariance violation through anomalies in the multi-TeV γ-ray spectra of blazars. *Astron. Astrophys.* **2016**, *585*, A25. [CrossRef]
26. Vercellone, S.; Bigongiari, C.; Burtovoi, A.; Cardillo, M.; Catalano, O.; Franceschini, A.; Lombardi, S.; Nava, L.; Pintore, F.; Stamerra, A.; et al. ASTRI Mini-Array core science at the Observatorio del Teide. *J. High Energy Astrophys.* **2022**, *35*, 1–42. [CrossRef]
27. CTAO. Available online: https://www.cta-observatory.org/ (accessed on 5 August 2025).
28. Egorov, A.E.; Topchiev, N.P.; Galper, A.M.; Dalkarov, O.D.; Leonov, A.A.; Suchkov, S.I.; Yurkin, Y.T. Dark matter searches by the planned gamma-ray telescope GAMMA-400. *JCAP* **2020**, *11*, 049. [CrossRef]
29. HAWC. Available online: https://www.hawc-observatory.org/ (accessed on 5 August 2025).
30. Huang, X.; Lamperstorfer, A.S.; Tsai, Y.-L.S.; Xu, M.; Yuan, Q.; Chang, J.; Dong, Y.; Hu, B.; Lü, J.; Wang, L.; et al. Perspective of monochromatic gamma-ray line detection with the High Energy cosmic-Radiation Detection (HERD) facility onboard China's space station. *Astropart. Phys.* **2016**, *78*, 35–42. [CrossRef]
31. Cao, Z.; della Volpe, D.; Liu, S.; Bi, X.; Chen, Y.; D'Ettorre Piazzoli, B. ; Feng, L. ; Jia, H.; Li, Z.; Ma, X.; et al. The Large High Altitude Air Shower Observatory (LHAASO) Science Book (2021 Edition). *Chin. Phys. C* **2022** *46*, 035001.
32. TAIGA-HiSCORE. Available online: https://taiga-experiment.info/taiga-hiscore/ (accessed on 5 August 2025).

33. Weisskopf, M.C.; Soffitta, P.; Baldini, L.; Ramsey, B.D.; O'Dell, S.L.; Romani, R.W.; Matt, G.; Deininger, W.D.; Baumgartner, W.H.; Bellazzini, R.; et al. Imaging X-ray Polarimetry Explorer: Prelaunch. *J. Astron. Telesc. Instruments Syst.* **2022**, *8*, 026002. [CrossRef]
34. Zhang, S.N.; Santangelo, A.; Xu, Y.; Feng, H.; Lu, F.; Chen, Y.; Ge, M.; Nandra, K.; Wu, X.; Feroci, M.; et al. The enhanced X-ray Timing and Polarimetry mission–eXTP. *Sci. China Phys. Mech. Astron.* **2019**, *62*, 29502. [CrossRef]
35. Abarr, Q.; Awaki, H.; Baring, M.G.; Bose, R.; Geronimo, G.D.; Dowkontt, P.; Errando, M.; Guarino, V.; Hattori, K.; Hayashida, K.; et al. XL-Calibur—a second-generation balloon-borne hard X-ray polarimetry mission. *Astropart. Phys.* **2021**, *126*, 102529. [CrossRef]
36. Soffitta, P.; Bucciantini, N.; Churazov, E.; Costa, E.; Dovciak, M.; Feng, H.; Heyl, J.; Ingram, A.; Jahoda, K.; Kaaret, P.; et al. A polarized view of the hot and violent universe. *Exp. Astron.* **2021**, *51*, 1109. [CrossRef]
37. Jahoda, K.; Krawczynski, H.; Kislat, F.; Marshall, H.; Okajima, T.; Agudo, I.; Angelini, L.; Bachetti, M.; Baldini, L.; Baring, M.; et al. The X-ray Polarization Probe mission concept. *arXiv* **2019**, arXiv:1907.10190. [CrossRef]
38. Yang, C.-Y.; Lowell, A.; Zoglauer, A.; Tomsick, J.; Chiu, J.-L.; Kierans, C.; Sleator, C.; Boggs, S.; Chang, H.-K.; Jean, P.; et al. The polarimetric performance of the Compton Spectrometer and Imager (COSI). *Proc. SPIE* **2018**, *10699*, 642.
39. De Angelis, A.; Tatischeff, V.; Tavani, M.; Oberlack, U.; Grenier, I.; Hanlon, L.; Walter, R.; Argan, A.; von Ballmoos, P.; Bulgarelli, A.; et al. The e-ASTROGAM mission. *Exp. Astron.* **2017**, *44*, 25–82. [CrossRef]
40. Tatischeff, V. et al. [e-ASTROGAM Collaboration]. The e-ASTROGAM gamma-ray space observatory for the multimessenger astronomy of the 2030s. *Proc. SPIE* **2018**, *10699*, 106992J.
41. Kierans, C.A. et al. [AMEGO Collaboration]. AMEGO: Exploring the Extreme Multimessenger Universe. *Proc. SPIE* **2020**, *11444*, 528–546.
42. Neronov, A.; Vovk, I. Evidence for Strong Extragalactic Magnetic Fields from Fermi Observations of TeV Blazars. *Science* **2010**, *328*, 73. [CrossRef]
43. Durrer, R.; Neronov, A. Cosmological magnetic fields: Their generation, evolution and observation. *A&AR* **2013**, *21*, 62.
44. Pshirkov, M.S.; Tinyakov, P.G.; Urban, F.R. New Limits on Extragalactic Magnetic Fields from Rotation Measures. *Phys. Rev. Lett.* **2016**, *116*, 191302. [CrossRef]
45. Ackermann, M.; Ajello, M.; Baldini, L.; Ballet, J.; Barbiellini, G.; Bastieri, D.; Bellazzini, R.; Bissaldi, E.; Blandford, R.D.; Bloom, E.D.; et al. The Search for Spatial Extension in High-latitude Sources Detected by the *Fermi* Large Area Telescope. *Astrophys. J. Suppl. Ser.* **2018**, *237*, 32. [CrossRef]
46. Tavecchio, F.; Ghisellini, G.; Foschini, L.; Bonnoli, G.; Ghirlanda, G.; Coppi, P. The intergalactic magnetic field constrained by *Fermi*/Large Area Telescope observations of the TeV blazar 1ES 0229+200. *Mon. Not. Astron. R. Soc.* **2010**, *406*, L70. [CrossRef]
47. Tavecchio, F.; Romano, P.; Landoni, M.; Vercellone, S. Putting the *hadron beam* scenario for extreme blazars to the test with the Cherenkov Telescope Array. *Mon. Not. Astron. R. Soc.* **2019**, *483*, 1802. [CrossRef]
48. Jaeckel, J.; Ringwald, A. The Low-Energy Frontier of Particle Physics. *Ann. Rev. Nucl. Part. Sci.* **2010**, *60*, 405–437. [CrossRef]
49. Ringwald, A. Exploring the role of axions and other WISPs in the dark universe. *Phys. Dark Univ.* **2012**, *1*, 116–135. [CrossRef]
50. Preskill, J.; Wise, M.B.; Wilczek, F. Cosmology of the invisible axion. *Phys. Lett. B* **1983**, *120*, 127–132. [CrossRef]
51. Abbott, L.F.; Sikivie, P. A cosmological bound on the invisible axion. *Phys. Lett. B* **1983**, *120*, 133–136. [CrossRef]
52. Dine, M.; Fischler, W. The not-so-harmless axion. *Phys. Lett. B* **1983**, *120*, 137–141. [CrossRef]
53. Arias, P.; Cadamuro, D.; Goodsell, M.; Jaeckel, J.; Redondo, J.; Ringwald, A. WISPy cold dark matter. *JCAP* **2012**, *013*, 008.
54. Kim, J.H. Light pseudoscalars, particle physics and cosmology. *Phys. Rep.* **1987**, *150*, 1–177. [CrossRef]
55. Cheng, H.Y. The strong CP problem revisited. *Phys. Rep.* **1988**, *158*, 1–89. [CrossRef]
56. Kim, J.E.; Carosi, G. Axions and the strong *CP* problem. *Rev. Mod. Phys.* **2010**, *82*, 557. [CrossRef]
57. Marsch, D.J.E. Axion cosmology. *Phys. Rep.* **2016**, *643*, 1. [CrossRef]
58. Heisenberg, W.; Euler, H. Folgerungen aus der diracschen theorie des positrons. *Z. Phys.* **1936**, *98*, 714–732. [CrossRef]
59. Weisskopf, V.S. Über die elektrodynamik des vakuums auf grund des quanten-theorie des elektrons. *K. Dan. Vidensk. Selsk. Mat. Fys. Medd.* **1936**, *14*, 6.
60. Schwinger, J. On Gauge Invariance and Vacuum Polarization. *Phys. Rev.* **1951**, *82*, 664. [CrossRef]
61. Dobrynina, A.; Kartavtsev, A.; Raffelt, G. Photon-photon dispersion of TeV gamma rays and its role for photon-ALP conversion. *Phys. Rev. D* **2015**, *91*, 083003; Erratum in *Phys. Rev. D* **2015**, *91*, 109902. [CrossRef]
62. CAST Collaboration. New CAST limit on the axion-photon interaction. *Nat. Phys.* **2017**, *13*, 584–590. [CrossRef]
63. Ayala, A.; Domínguez, I.; Giannotti, M.; Mirizzi,A.; Straniero, O. Revisiting the Bound on Axion-Photon Coupling from Globular Clusters. *Phys. Rev. Lett.* **2014**, *113*, 191302. [CrossRef]
64. Payez, A.; Evoli, C.; Fischer, T.; Giannotti, M.; Mirizzi, A.; Ringwald, A. Revisiting the SN1987A gamma-ray limit on ultralight axion-like particles. *JCAP* **2015**, *02*, 006. [CrossRef]
65. Ajello, M. et al. [Fermi-LAT collaboration]. Search for spectral irregularities due to photon-axionlike-particle oscillations with the Fermi Large Area Telescope. *Phys. Rev. Lett.* **2016**, *116*, 161101. [CrossRef]

66. Berg, M.; Conlon, J.P.; Day, F.; Jennings, N.; Krippendorf, S.; Powell, A.J.; Rummel, M. Constraints on axion-like particles from X-ray observations of NGC1275. *Astrophys. J.* **2017**, *847*, 101. [CrossRef]
67. Conlon, J.P.; Day, F.; Jennings, N.; Krippendorf, S.; Rummel, M. Constraints on axion-like particles from non-observation of spectral modulations for X-ray point sources. *JCAP* **2017**, *07*, 005. [CrossRef]
68. Meyer, M.; Petrushevska, T. et al. [Fermi-LAT Collaboration]. Search for Axionlike-Particle-Induced Prompt γ-Ray Emission from Extragalactic Core-Collapse Supernovae with the *Fermi* Large Area Telescope. *Phys. Rev. Lett.* **2020**, *124*, 231101; Erratum in *Phys. Rev. Lett.* **2020**, *125*, 119901. [CrossRef]
69. Reynolds, C.S.; Marsh, M.C.D.; Russell, H.R.; Fabian, A.C.; Smith, R.; Tombesi, F.; Veilleux, S. Astrophysical limits on very light axion-like particles from Chandra grating spectroscopy of NGC 1275. *Astrophys. J.* **2020**, *890*, 59. [CrossRef]
70. Sisk-Reynés, J.; Matthews, J.H.; Reynolds, C.S.; Russell, H.R.; Smith, R.N.; Marsh, M.C.D. New constraints on light axion-like particles using *Chandra* transmission grating spectroscopy of the powerful cluster-hosted quasar H1821+643. *Mon. Not. Astron. R. Soc.* **2022**, *510*, 1264. [CrossRef]
71. Schallmoser, S.; Krippendorf, S.; Chadha-Day, F.; Weller, J. Updated Bounds on Axion-Like Particles from X-ray Observations. *Mon. Not. Astron. R. Soc.* **2022**, *514*, 329. [CrossRef]
72. Matthews, J.H.; Reynolds, C.S.; Marsh, M.C.D.; Sisk-Reynés, J.; Rodman, P.E. How do Magnetic Field Models Affect Astrophysical Limits on Light Axion-like Particles? An X-ray Case Study with NGC 1275. *Astrophys. J.* **2022**, *930*, 90. [CrossRef]
73. Dessert, C.; Dunsky, D.; Safdi, B.R. Upper limit on the axion-photon coupling from magnetic white dwarf polarization. *Phys. Rev. D* **2022**, *105*, 103034. [CrossRef]
74. Maiani, L.; Petronzio, R.; Zavattini, E. Effects of nearly massless, spin-zero particles on light propagation in a magnetic field. *Phys. Let. B* **1986**, *175*, 359–363. [CrossRef]
75. Raffelt, G.G.; Stodolsky, L. Mixing of the photon with low-mass particles. *Phys. Rev. D* **1988**, *37*, 1237. [CrossRef]
76. De Angelis, A.; Roncadelli, M.; Mansutti, O. Evidence for a new light spin-zero boson from cosmological gamma-ray propagation? *Phys. Rev. D* **2007**, *76*, 121301. [CrossRef]
77. Simet, M.; Hooper, D.; Serpico, P.D. Milky Way as a kiloparsec-scale axionscope. *Phys. Rev. D* **2008**, *77*, 063001. [CrossRef]
78. Sánchez-Conde, M.A.; Paneque, D.; Bloom, E.; Prada, F.; Domínguez, A. Hints of the existence of axionlike particles from the gamma-ray spectra of cosmological sources. *Phys. Rev. D* **2009**, *79*, 123511. [CrossRef]
79. De Angelis, A.; Galanti, G.; Roncadelli, M. Relevance of axionlike particles for very-high-energy astrophysics. *Phys. Rev. D* **2011**, *84*, 105030; Erratum in *Phys. Rev. D* **2013**, *87*, 109903. [CrossRef]
80. Tavecchio, F.; Roncadelli, M.; Galanti, G.; Bonnoli, G. Evidence for an axion-like particle from PKS 1222+216? *Phys. Rev. D* **2012**, *86*, 085036. [CrossRef]
81. Wouters, D.; Brun, P. Irregularity in gamma ray source spectra as a signature of axionlike particles. *Phys. Rev. D* **2012**, *86*, 043005. [CrossRef]
82. Tavecchio, F.; Roncadelli, M.; Galanti, G. Photons to axion-like particles conversion in Active Galactic Nuclei. *Phys. Lett. B* **2015**, *744*, 375–379. [CrossRef]
83. Kohri, K.; Kodama, H. Axion-like particles and recent observations of the cosmic infrared background radiation. *Phys. Rev. D* **2017**, *96*, 051701. [CrossRef]
84. Galanti, G.; Tavecchio, F.; Roncadelli, M.; Evoli, C. Blazar VHE spectral alterations induced by photon–ALP oscillations. *Mon. Not. Astron. R. Soc.* **2019**, *487*, 123. [CrossRef]
85. Galanti, G.; Roncadelli, M.; De Angelis, A.; Bignami, G.F. Hint at an axion-like particle from the redshift dependence of blazar spectra. *Mon. Not. Astron. R. Soc.* **2020**, *493*, 1553. [CrossRef]
86. Galanti, G.; Nava, L.; Roncadelli, M.; Tavecchio, F.; Bonnoli, G. Observability of the Very-High-Energy Emission from GRB 221009A. *Phys. Rev. Lett.* **2023**, *131*, 251001. [CrossRef] [PubMed]
87. Jain, P.; Panda, S.; Sarala, S. Electromagnetic polarization effects due to axion-photon mixing. *Phys. Rev. D* **2002**, *66*, 085007. [CrossRef]
88. Bassan, N.; Mirizzi, A.; Roncadelli, M. Axion-like particle effects on the polarization of cosmic high-energy gamma sources. *JCAP* **2010**, *5*, 010. [CrossRef]
89. Agarwal, N.; Kamal, A.; Jain, P. Alignments in quasar polarizations: Pseudoscalar-photon mixing in the presence of correlated magnetic fields. *Phys. Rev. D* **2011**, *83*, 065014. [CrossRef]
90. Payez, A.; Cudell, J.R.; Hutsemekers, D. Can axionlike particles explain the alignments of the polarizations of light from quasars? *Phys. Rev. D* **2011**, *84*, 085029. [CrossRef]
91. Agarwal, N.; Aluri, P.K.; Jain, P.; Khanna, U.; Tiwari, P. A complete 3D numerical study of the effects of pseudoscalar-photon mixing on quasar polarizations. *Eur. Phys. J. C* **2012**, *72*, 1928. [CrossRef]
92. Perna, R.; Ho, W.C.G.; Verde, L.; Adelsberg, M. Jimenez, R. Signatures of photon-axion conversion in the thermal spectra and polarization of neutron stars. *Astrophys. J.* **2012**, *748*, 116. [CrossRef]
93. Day, F.; Krippendorf, S. Searching for axion-like particles with X-ray polarimeters. *Galaxies* **2018**, *6*, 45. [CrossRef]

94. Galanti, G. Photon-ALP interaction as a measure of initial photon polarization. *Phys. Rev. D* **2022**, *105*, 083022. [CrossRef]
95. Galanti, G. Photon-ALP oscillations inducing modifications to photon polarization. *Phys. Rev. D* **2023**, *107*, 043006. [CrossRef]
96. Galanti, G.; Roncadelli, M.; Tavecchio, F.; Costa, E. ALP induced polarization effects on photons from galaxy clusters. *Phys. Rev. D* **2023**, *107*, 103007. [CrossRef]
97. Galanti, G.; Roncadelli, M.; Tavecchio, F. ALP-induced polarization effects on photons from blazars. *Phys. Rev. D* **2023**, *108*, 083017. [CrossRef]
98. Wheeler, J.A. *Geometrodynamics*; Academic Press: London, UK, 1962.
99. Wheeler, J.A. *Relativity, Groups and Topology*; Dewitt, M.C., Dewitt, B.S., Eds.; Gordon and Breach: New York, NY, USA, 1964.
100. Hawking, S.W. Spacetime foam. *Nucl. Phys. B* **1978**, *144*, 349. [CrossRef]
101. Carlip, S. Spacetime Foam and the Cosmological Constant. *Phys. Rev. Lett.* **1997**, *79*, 4071. [CrossRef]
102. Garay, L.J. Spacetime Foam as a Quantum Thermal Bath. *Phys. Rev. Lett.* **1998**, *80*, 2508. [CrossRef]
103. Garay, L.J. Thermal properties of spacetime foam. *Phys. Rev. D* **1998**, *58*, 124015. [CrossRef]
104. Liberati, S. Tests of Lorentz invariance: A 2013 update. *Class. Quant. Grav.* **2013**, *30*, 133001. [CrossRef]
105. Albert, A.; Alfaro, R.; Alvarez, C.; Camacho, J.R.A.; Arteaga-Velázquez, J.C.; Arunbabu, K.P.; Rojas, D.A.; Solares, H.A.A.; Baghmanyan, V.; Belmont-Moreno, E.; et al. Constraints on Lorentz Invariance Violation from HAWC Observations of Gamma Rays above 100 TeV. *Phys. Rev. Lett.* **2020**, *124*, 131101. [CrossRef]
106. Li, C.; Ma, B.-Q. Ultrahigh-energy photons from LHAASO as probes of Lorentz symmetry violations. *Phys. Rev. D* **2021**, *104*, 063012. [CrossRef]
107. Li, H.; Ma, B.-Q. Lorentz invariance violation induced threshold anomaly versus very-high energy cosmic photon emission from GRB 221009A. *Astropart. Phys.* **2023**, *148*, 102831. [CrossRef]
108. Finke, J.D.; Razzaque, S. Possible Evidence for Lorentz Invariance Violation in Gamma-Ray Burst 221009A. *Astrophys. J.* **2023**, *942*, L21. [CrossRef]
109. Yang, Y.-M.; Bi, X.-J.; Yin, P.-F. Constraints on Lorentz invariance violation from the LHAASO observation of GRB 221009A. *JCAP* **2024**, *04*, 060. [CrossRef]
110. Piran, T.; Ofengeim, D.D. Lorentz invariance violation limits from GRB 221009A. *Phys. Rev. D* **2024**, *109*, L081501. [CrossRef]
111. Cao, Z. et al. [LHAASO Collaboration]. Stringent Tests of Lorentz Invariance Violation from LHAASO Observations of GRB 221009A. *Phys. Rev. Lett.* **2024**, *133*, 071501. [CrossRef] [PubMed]
112. Galanti, G.; Roncadelli, M. Is Lorentz invariance violation found? *arXiv* **2025**, arXiv:2504.01830. [CrossRef]
113. Stecker, F.W.; Glashow, S.L. New tests of Lorentz invariance following from observations of the highest energy cosmic γ-rays. *Astropart. Phys.* **2001**, *16*, 97. [CrossRef]
114. Galanti, G.; Tavecchio, F.; Landoni, M. Fundamental physics with blazar spectra: A critical appraisal. *Mon. Not. Astron. R. Soc.* **2020**, *491*, 5268. [CrossRef]
115. Aharonian, F.A. et al. [HEGRA Collaboration]. Reanalysis of the high energy cutoff of the 1997 Mkn 501 TeV energy spectrum. *Astron. Astrophys.* **2001**, *366*, 62. [CrossRef]
116. Aharonian, F.A. et al. [HESS Collaboration]. New constraints on the mid-IR EBL from the HESS discovery of VHE γ-rays from 1ES 0229+200. *Astron. Astrophys.* **2007**, *475*, L9. [CrossRef]
117. Aliu, E.; Archambault, S.; Arlen, T.; Aune, T.; Behera, B.; Beilicke, M.; Benbow, W.; Berger, K.; Bird, R.; Bouvier, A.; et al. A Three-year Multi-wavelength Study of the Very-high-energy γ-Ray Blazar 1ES 0229+200. *Astrophys. J.* **2014**, *782*, 13. [CrossRef]
118. Costamante, L.; Bonnoli, G.; Tavecchio, F.; Ghisellini, G.; Tagliaferri, G.; Khangulyan, D. The *NuSTAR* view on hard-TeV BL Lacs. *Mon. Not. Astron. R. Soc.* **2018**, *477*, 4257. [CrossRef]
119. Cerruti, M.; Zech, A.; Boisson, C.; Inoue, S. A hadronic origin for ultra-high-frequency-peaked BL Lac objects. *Mon. Not. Astron. R. Soc.* **2015**, *448*, 910. [CrossRef]
120. Zhang, H.; Böttcher, M. X-Ray and Gamma-Ray Polarization in Leptonic and Hadronic Jet Models of Blazars. *Astrophys. J.* **2013**, *774*, 18. [CrossRef]
121. Böttcher, M.; Reimer, A.; Sweeney, K.; Prakash, A. Leptonic and Hadronic Modeling of Fermi-detected Blazars. *Astrophys. J.* **2013**, *768*, 54. [CrossRef]
122. Di Gesu, L.; Donnarumma, I.; Tavecchio, F.; Agudo, I.; Barnounin, T.; Cibrario, N.; Lalla, N.D.; Marco, A.D.; Escudero, J.; Errando, M.; et al. The X-Ray Polarization View of Mrk 421 in an Average Flux State as Observed by the Imaging X-Ray Polarimetry Explorer. *Astrophys. J. Lett.* **2022**, *938*, L7. [CrossRef]
123. Liodakis, I.; Marscher, A.P.; Agudo, I.; Berdyugin, A.V.; Bernardos, M.I.; Bonnoli, G.; Borman, G.A.; Casadio, C.; Casanova, V.; Cavazzuti, E.; et al. Polarized blazar X-rays imply particle acceleration in shocks. *Nature* **2022**, *611*, 677. [CrossRef] [PubMed]
124. Middei, R.; Liodakis, I.; Perri, M.; Puccetti, S.; Cavazzuti, E.; Gesu, L.D.; Ehlert, S.R.; Madejski, G.; Marscher, A.P.; Marshall, H.L.; et al. X-Ray Polarization Observations of BL Lacertae. *Astrophys. J. Lett.* **2023**, *942*, L10. [CrossRef]
125. Peirson, A.L.; Negro, M.; Liodakis, I.; Middei, R.; Kim, D.E.; Marscher, A.P.; Marshall, H.L.; Pacciani, L.; Romani, R.W.; Wu, K.; et al. X-Ray Polarization of BL Lacertae in Outburst. *Astrophys. J. Lett.* **2023**, *948*, L25. [CrossRef]

126. Middei, R.; Perri, M.; Puccetti, S.; Liodakis, I.; Gesu, L.D.; Marscher, A.P.; Cavero, N.R.; Tavecchio, F.; Donnarumma, I.; Laurenti, M.; et al. IXPE and Multiwavelength Observations of Blazar PG 1553+113 Reveal an Orphan Optical Polarization Swing. *Astrophys. J. Lett.* **2023**, *953*, L28. [CrossRef]
127. Ehlert, S.R.; Liodakis, I.; Middei, R.; Marscher, A.P.; Tavecchio, F.; Agudo, I.; Kouch, P.M.; Lindfors, E.; Nilsson, K.; Myserlis, I.; et al. X-Ray Polarization of the BL Lacertae Type Blazar 1ES 0229+200. *Astrophys. J.* **2023**, *959*, 61. [CrossRef]
128. Di Gesu, L.; Marshall, H.L.; Ehlert, S.R.; Kim, D.E.; Donnarumma, I.; Tavecchio, F.; Liodakis, I.; Kiehlmann, S.; Agudo, I.; Jorstad, S.G.; et al. Discovery of X-ray polarization angle rotation in the jet from blazar Mrk 421. *Nat. Astron.* **2023**, *7*, 1245. [CrossRef]
129. Errando, M.; Liodakis, I.; Marscher, A.P.; Kim, D.E.; Donnarumma, I.; Tavecchio, F.; Liodakis, I.; Kiehlmann, S.; Agudo, I.; Jorstad, S.G.; et al. Detection of X-Ray Polarization from the Blazar 1ES 1959+650 with the Imaging X-Ray Polarimetry Explorer. *Astrophys. J.* **2024**, *963*, 5. [CrossRef]
130. Kouch, P.M.; Liodakis, I.; Middei, R.; Kim, D.E.; Tavecchio, F.; Marscher, A.P.; Marshall, H.L.; Ehlert, S.R.; Gesu, L.D.; Jorstad, S.G.; et al. IXPE observation of PKS 2155-304 reveals the most highly polarized blazar. *arXiv* **2024**, arXiv:2406.01693. [CrossRef]
131. Zhang, H.; Böttcher, M.; Liodakis, I. Revisiting High-Energy Polarization from Leptonic and Hadronic Blazar Scenarios. *arXiv* **2024**, arXiv:2404.12475. [CrossRef]
132. Kostelecký, V.A.; Mewes, M. Electrodynamics with Lorentz-violating operators of arbitrary dimension. *Phys. Rev. D* **2009**, *80*, 015020. [CrossRef]
133. Kislat, F.; Krawczynski, H. Planck-scale constraints on anisotropic Lorentz and *CPT* invariance violations from optical polarization measurements. *Phys. Rev. D* **2017**, *95*, 083013. [CrossRef]
134. Friedman, A.S.; Leon, D.; Crowley, K.D.; Johnson, D.; Teply, G.; Tytler, D.; Keating, B.G.; Cole, G.M. Constraints on Lorentz Invariance and *CPT* Violation using Optical Photometry and Polarimetry of Active Galaxies BL Lacertae and S5 B0716+714. *Phys. Rev. D* **2019**, *99*, 035045. [CrossRef]
135. Kislat, F. Searches for Lorentz-Violating Signals with Astrophysical Polarization Measurements. In Proceedings of the 8th Meeting on CPT and Lorentz Symmetry (CPT'19), Bloomington, IN, USA, 12–16 May 2019; pp. 162–165.